CHIN. PHYS. LETT. Vol. 32, No. 11 (2015) 114203

Effects of Finite Surface on Polarization State of Thermal Emission *

LIU Fei(刘飞), SHAO Xiao-Peng(邵晓鹏)**, XIANGLI Bin(相里斌), GAO Ying(高鹰),
HAN Ping-Li(韩平丽), WANG Lin(王琳)

School of Physics and Optoelectronic Engineering, Xidian University, Xi'an 710071

(Received 6 July 2015)

A comprehensive model for explaining the polarization properties of thermal emission is presented for the case of objects with certain sizes. Using Stokes theory and the superposition principle of a light wave, we analyze the dependence of degree of linear polarization on the spatial geometrical relations including the sizes of objects, the detection distance, and the locations of objects for both metallic and nonmetallic objects, each taken separately.

PACS: 42.25.Ja, 52.25.Os, 77.22.Ej DOI: 10.1088/0256-307X/32/11/114203

Polarization is a physical signature of light that can be exploited for improving the target recognition probability of optical detection systems.[1–3] Polarization characteristics of infrared thermal emission are used by many researchers since these characteristics depend on thermal emission rather than reflected light and they are relatively unaffected by illumination changes in visible wave bands.[4,5] A number of investigations have been carried out to prove that the polarization states of thermal emission represent the inherent information of objects, for example, the thermal radiation emitted by metallic and nonmetallic objects exhibit different linear polarization states.[6] This kind of polarization is thought to originate from the anisotropy generated by the superposition of elemental thermal radiators located near the surface-air interface of a material.[7] As the foundation of detection, ways to measure polarization states of thermal emission have been widely studied.[8] The framework of Fresnel theory and Kirchhoff's law explained the polarization characteristics of thermal radiation emitted by point source.[9,10] More studies have concentrated on the effect of surface roughness on the degree of linear polarization (DOLP) of thermal emission in some specific wave bands.[11,12]

The model regarding radiation sources as points is a highly idealized situation without considerations of any other factors, in that case only the refractive indexes of different materials take effect. Studies in relation between surface roughness and DOLP of thermal emission reveal that the polarization states of thermal emission contain geometrical information of the emitting surface. So far, there have been few particular investigations on how the polarization states of thermal emission are affected by the spatial geometrical relations, including the sizes of objects, the detection distance, and the locations of objects. In this Letter, a comprehensive model regarding objects as radiation sources with specific sizes is presented, which emphasizes the measurements of DOLP values of thermal emission when the spatial geometrical relation changes with the long-infrared wave bands. In brief, we call this proposed model a finite surface model (FSM). As described by the FSM, the polarization state of thermal emission differs much from that in the point source model (PSM), with providing useful and accurate information to exhibit the surface's polarization signature objectively.

This work starts with the Stokes theory which uses four parameters s_0, s_1, s_2 and s_3 to describe polarization states of thermal emission as[13,14]

$$S = \begin{bmatrix} s_0 \\ s_1 \\ s_2 \\ s_3 \end{bmatrix} = \begin{bmatrix} \langle |E_x|^2 + |E_y|^2 \rangle \\ \langle |E_x|^2 - |E_y|^2 \rangle \\ 2\mathrm{Re}\langle E_x E_y^* \rangle \\ -2\mathrm{Im}\langle E_x E_y^* \rangle \end{bmatrix} = \begin{bmatrix} I_{0^\circ} + I_{90^\circ} \\ I_{0^\circ} - I_{90^\circ} \\ I_{45^\circ} - I_{135^\circ} \\ I_{\mathrm{L}} - I_{\mathrm{R}} \end{bmatrix}, \quad (1)$$

where s_0 is the total intensity of radiation, s_1 describes the preponderance of linearly horizontal polarized radiation over linearly vertical polarized radiation, s_2 stands for the preponderance of linearly $+45^\circ$ polarized radiation over linearly $+135^\circ$ polarized radiation, and s_3 denotes the preponderance of left circularly polarized radiation over right circularly polarized radiation, I_α (α is 0°, 45°, 90°, or 135°) is the intensity of radiation transmitted across a linear polarizer oriented at an angle α between the transmission axis of the polarizer and the axis x_0. Generally, s_3 is ignored in most cases, since polarization detectors are blind to almost all the circular polarization states. DOLP, the fraction of the intensity attributed by linear polarized light, can be calculated in terms of the Stokes Vector[15]

$$\mathrm{DOLP} = \frac{\sqrt{s_1^2 + s_2^2}}{s_0}. \quad (2)$$

Based on the Stokes theory, the FSM is proposed. It starts with the assumption that a radiation source with a specific size could be treated as a collection of numerous points that are independent of each other. As shown in Fig. 1, Q stands for the view point which is set at Z-axis, plane ABCD denotes the radiation

*Supported by the Fundamental Research Funds for the Central Universities under Grant No NSIY021402
**Corresponding author. Email: xpshao@xidian.edu.cn
© 2015 Chinese Physical Society and IOP Publishing Ltd

source, and $O'(x', y', 0)$ is an arbitrary point on the object. Take $O'(x', y', 0)$ as an example, the emission could be separated to two orthogonal directions, usually written as the p-direction and s-direction. This depicts the components of light vector E_p and E_s given in Fig. 1.[16,17] Due to the fact that the electric vector vibrates asymmetrically relative to its direction of propagation, the detected emission could not be equally separated to p-direction and s-direction. In other words, the detected emission is polarized. As to the whole surface (plane ABCD) of the object shown in Fig. 1, its DOLP values could be calculated in combination with the superposition principle of a light wave. The detailed calculation model of DOLP of thermal emission is given by

$$
\begin{aligned}
I_{0^\circ} &= \int_{x_1}^{x_2}\int_{y_1}^{y_2}\left[\frac{\varepsilon_\mathrm{s}}{\cos\theta}\cdot\sin\varphi+\varepsilon_\mathrm{p}\cos\varphi\right]\\
&\quad\cdot\left[\frac{\|E\|^2}{2-\rho_\mathrm{s}-\rho_\mathrm{p}}\right]dxdy,\\
I_{45^\circ} &= \int_{x_1'}^{x_2'}\int_{f_1(x)}^{f_2(x)}\left[\frac{\varepsilon_\mathrm{s}}{\cos\theta}\cdot\cos\varphi+\varepsilon_\mathrm{p}\sin\varphi\right]\\
&\quad\cdot\left[\frac{\|E\|^2}{2-\rho_\mathrm{s}-\rho_\mathrm{p}}\right]dxdy\\
&\quad+\int_{x_2'}^{x_3'}\int_{f_3(x)}^{f_4(x)}\left[\frac{\varepsilon_\mathrm{s}}{\cos\theta}\cdot\cos\varphi+\varepsilon_\mathrm{p}\sin\varphi\right]\\
&\quad\cdot\left[\frac{\|E\|^2}{2-\rho_\mathrm{s}-\rho_\mathrm{p}}\right]dxdy,\\
I_{90^\circ} &= \int_{x_1}^{x_2}\int_{y_1}^{y_2}\left[\frac{\varepsilon_\mathrm{s}}{\cos\theta}\cdot\cos\varphi+\varepsilon_\mathrm{p}\sin\varphi\right]\\
&\quad\cdot\left[\frac{\|E\|^2}{2-\rho_\mathrm{s}-\rho_\mathrm{p}}\right]dxdy,\\
I_{135^\circ} &= \int_{x_1'}^{x_2'}\int_{f_1(x)}^{f_2(x)}\left[\frac{\varepsilon_\mathrm{s}}{\cos\theta}\cdot\sin\varphi+\varepsilon_\mathrm{p}\cos\varphi\right]\\
&\quad\cdot\left[\frac{\|E\|^2}{2-\rho_\mathrm{s}-\rho_\mathrm{p}}\right]dxdy\\
&\quad+\int_{x_2'}^{x_3'}\int_{f_3(x)}^{f_4(x)}\left[\frac{\varepsilon_\mathrm{s}}{\cos\theta}\cdot\sin\varphi+\varepsilon_\mathrm{p}\cos\varphi\right]\\
&\quad\cdot\left[\frac{\|E\|^2}{2-\rho_\mathrm{s}-\rho_\mathrm{p}}\right]dxdy. \qquad (3)
\end{aligned}
$$

The bounds in Eq. (3) are determined by

$$
\begin{aligned}
f_1(x) &= (-x)+\frac{x_1}{\cos(\pi/4)},\quad f_2(x)=x+\frac{y_2}{2\cdot\cos(\pi/4)},\\
f_3(x) &= x+\frac{y_1}{2\cdot\cos(\pi/4)},\quad f_4(x)=(-x)+\frac{x_2}{\cos(\pi/4)}, \qquad (4)
\end{aligned}
$$

and

$$
\begin{aligned}
x_1' &= x_1\cdot\cos(\pi/4)-y_2\cdot\sin(\pi/4),\\
x_2' &= x_1\cdot\cos(\pi/4)-y_1\cdot\sin(\pi/4),\\
x_3' &= x_2\cdot\cos(\pi/4)-y_1\cdot\sin(\pi/4), \qquad (5)
\end{aligned}
$$

where ε and ρ are the directional emissivity and directional hemispherical intensity reflectivity of an object, respectively.[18] Emissivity is a number that varies from zero to one, which describes how efficiently an object radiates thermal radiation. According to the Kirchhoff law, the emissivity of a material equates to the absorption coefficient by consideration of a material in equilibrium, and this result has been extended to non-equilibrium conditions. For a uniform and isotropic opaque body $\varepsilon = 1-\rho$. Following convention, the emission could be separated to p-direction and s-direction, correspondingly, p-emissivity and s-emissivity exist as expressed by

$$
\varepsilon_\mathrm{p} = 1-\rho_\mathrm{p},\quad \varepsilon_\mathrm{s} = 1-\rho_\mathrm{s}. \qquad (6)
$$

If the complex refractive index of the material is known, then for a smooth surface, ρ_p and ρ_s can be calculated by using the Fresnel equations. Hence, Stokes vector can be obtained utilizing Eqs. (1) and (3), and this vector will then be used to calculate DOLP values by Eq. (2).

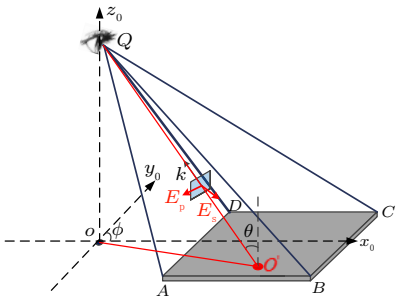


Fig. 1. Geometry for computation of DOLP values of thermal emission from a finite surface. Plane ABCD is a finite surface and coordinates of A, B, C and D are (x_1, y_1, 0), (x_2, y_1, 0), (x_2, y_2, 0) and (x_1, y_2, 0), respectively. The coordinate of the view point Q is (0, 0, z).

Employing the presented model, DOLP values of four materials, aluminum, iron, sand and A2059 glass, are obtained to make verification. Firstly, take square targets with the size of 4 m × 4 m as an example, and set their centers at (288, 0, 0) in the coordinate system. Secondly, calculate the intensities in directions of 0°, 45°, 90° and 135° by Eq. (3) as well as the complex refractive indexes of four materials at wavelength of 8 μm (considering that at the normal temperature, the wavelength of objects' emission locates at about the wavelength of 8 μm, thus we take the wavelength of 8 μm as an example), and then substitute the results (I_0, I_{45}, I_{90}, and I_{135}) into Eq. (2). Employing this equation, we obtain the DOLP values as shown in Fig. 2. It is worth noting that Fig. 2 shows the data within the distance of 300 m (in this work we take the distance from the viewer point to the origin as the detection distance for simplifying the calculations). When the distance is more than 300 m, DOLP values of objects with the size of 4 m × 4 m should be calculated by employing the PSM. In other words, the FSM is suitable for objects that cannot be handled as point

sources. Taking the iron as an example, there exists a critical point H_2 in Fig. 2, and after reaching this point the PSM should be employed. In particular, the selection of the critical point is based on the relation between extended radiation source and point radiation source.[20] In more detail, at the distance of 300 m, the emission angle is about 45°, and the DOLP values calculated are in agreement with the result of the PSM at the 45° emission angle. For instance, in the FSM, the DOLP values of aluminum, iron, sand and A2059 glass are 0.46, 0.41, 0.12 and 0.09 when the object is placed at the distance of 300 m. Correspondingly, in the PSM, the DOLP values of these four objects are 0.412, 0.408, 0.18 and 0.142 when the emission angle is 45°. At distances greater than 300 m, the object could be approximated as a point source. Furthermore, as can be clearly seen in Fig. 2, the DOLP values of the four materials behave similarly in their overall trends, while specific values differ from each other, especially between metal and nonmetal. Another feature of the curves in Fig. 2 that deserves special attention is the inflection point M. Detailed explanation of M is listed in the following since it is rather the matter to induce FSM distinguished from PSM.

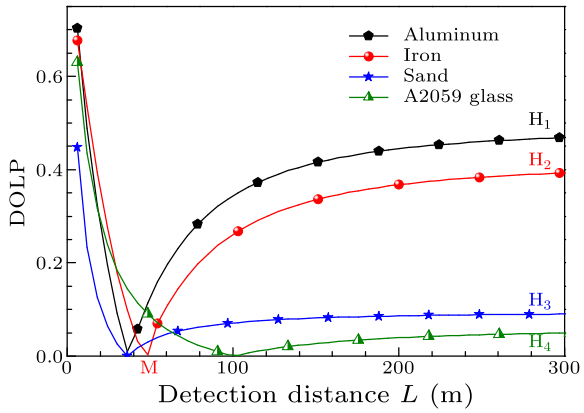


Fig. 2. DOLP values of four materials with the size of 4 m × 4 m calculated by FSM. Complex refractive indexes of these materials at the wavelength of 8 μm are 22.19+i82.83 (Al), 7.07+i27.9 (Fe), 2.81+i0.53 (Sand) and 1.97+i0.76 (A2059) according to Ref. [19].

We still take the iron as an example, and the Stokes theory can be used to explain the inflection point. First, the intensities of the four directions (0°, 45°, 90° and 135°) are calculated, as shown in Fig. 3, in which the intensity at 45° is almost the same as that at 135°. According to Eqs. (1) and (2), DOLP is determined only by intensities at 0° and 90° at this point. Then, the intensity difference between $I_{0°}$ and $I_{90°}$ is calculated, as shown in Fig. 3(b). Two features should be noticed in Fig. 3(b), one is that both positive and negative values exist, which indicates the disequilibrium of intensity in the two directions; the other is that when the intensity difference reaches zero, it would lead to the existence of the inflection point M, and should be regarded as the transformation of polarization type (p-polarization converts to s-polarization).

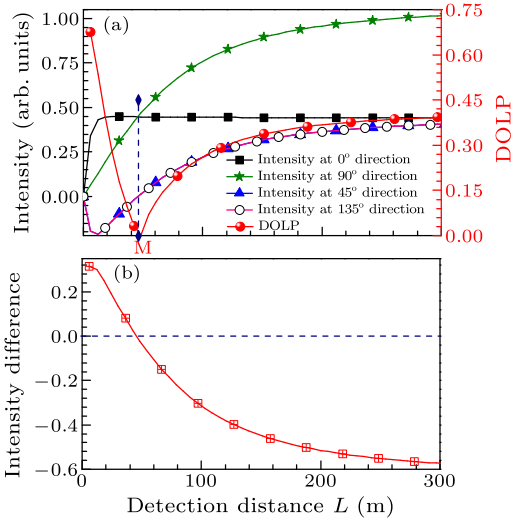


Fig. 3. (a) DOLP values and thermal emission intensities in four directions, 0°, 45°, 90° and 135°, of iron material with the size of 4 m × 4 m. (b) Difference between the intensities at 0° and 90° shown in Fig. 3(a).

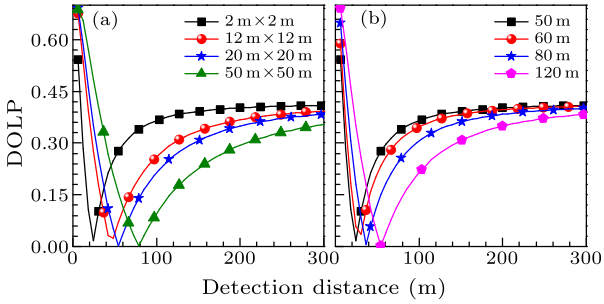


Fig. 4. (a) Range of DOLP values of iron objects located at the same location with sizes of 2 m × 2 m, 12 m × 12 m, 20 m × 20 m and 50 m × 50 m. (b) Range of DOLP values of an iron object with the size of 4 m × 4 m located at four different locations, whose starting points x_1 are 50, 60, 80 and 120 m, respectively.

The FSM emphasizes demonstration of the effects of objects' sizes as well as the detection distances on DOLP. Taking iron material as an example, Fig. 4(a) demonstrates the range of DOLP values of objects at the same location (the starting point x_1 is 250 m) while with different sizes of 2 m × 2 m, 12 m × 12 m, 20 m × 20 m and 50 m × 50 m. The results indicate similar changing trends of DOLP values, while in that case it needs a farther detection distance for a larger object to reach the same DOLP value as a smaller one. Figure 4(b) shows the DOLP values of the fixed-size object (4 m × 4 m) at various positions (starting points x_1 are 50, 60, 80 and 120 m, respectively). As can be seen in Fig. 4(b), there is an obvious trend that the DOLP values decrease with the increase of starting point coordinates x_1 with the same detection distance. As an example, when the detection distance becomes 150 m, the DOLP value (0.38) of the black curve ($x_1 = 50$ m) is 1.73 times larger than that (0.22) of the pink curve ($x_1 = 120$ m). On the whole, the curves of DOLP values are similar in their trends, whereas differences arise between objects with different sizes or

locations.

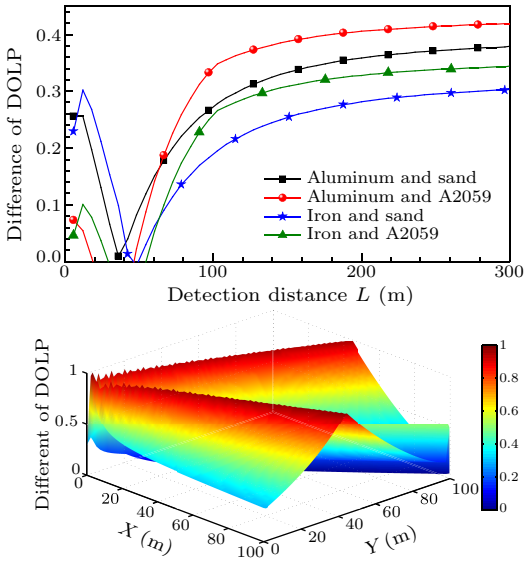


Fig. 5. Difference of DOLP values between objects of different materials. (a) Difference of DOLP values between aluminum and sand, aluminum and A2059, iron and sand as well as iron and A2059. (b) Difference of DOLP values between iron and sand when the viewer point is fixed while objects are moved in the first quadrant.

After characterizing DOLP as an index to distinguish different matter of various materials, we calculate DOLP differences between different materials, as shown in Fig. 5. In Fig. 5(a), the following four cases, i.e., DOLP differences between aluminum and sand, between aluminum and A2059, between iron and sand, and between iron and A2059, are thoroughly analyzed. The objects with the same size of 4 m × 4 m are fixed on plane ABCD with the starting point of $x_1 = 250$, $y_1 = -2$. The results are indicative of DOLP differences of various objects that objectively exist. As a more specific example, Fig. 5(b) shows the variation of DOLP difference between iron and sand at a 300 m detection distance when objects are moved in the first quadrant area (shown in Fig. 1). As can be seen, the differences of DOLP values are generally noticeable despite objects' different locations. Moreover, DOLP changes nonlinearly, which is not as speculated by researchers as linear. On the whole, DOLP characteristics can always be employed to distinguish objects of different materials wherever they are located. In addition, we could find a best detection distance based on the results provided by the FSM when distinguishing various materials.

In summary, the FSM, laying stress on analyzing polarization characteristics of objects that could not be approximated as point sources, is proposed. The formula for DOLP of a certain object is consistent with the results put forward in the literature,[11] and the numerical values are found to demonstrate the dependence of physical polarization behavior of objects on the spatial geometrical relations including the sizes of objects, the detection distance, and the locations of objects. Understanding of this kind of polarization properties of objects enables access to distinguishing among objects of different materials and an optimized observing position in practice. Furthermore, the FSM is also capable of characterizing polarization characteristics of three-dimensional space objects. Since two-dimensional planes are approximated as a single surface, three-dimensional objects should be approximated as multiple surfaces. Their polarization characteristics can be presented by relatively more complicated calculations.

Future work may extend to investigate the polarization states of thermal emission of objects with limited sizes and roughened or microcontoured surfaces. Comprehension of polarization characteristics of various objects should greatly improve if the depolarization effect could be taken into consideration. We hope our analysis inspires related studies of polarization properties especially in applying them to target detection and recognition.

We would like to thank Professor Wang Xueen for helpful discussions, Gong Rui, Kong Qinglin and Yang Cindy for checking the English grammar of this article.

References

[1] Denis G et al 2014 *Opt. Lett.* **39** 5768
[2] Chen H Y et al 2015 *Chin. Phys.* B **24** 014201
[3] Bao Y J et al 2014 *Chin. Phys.* B **23** 104218
[4] Alex J Y et al 2014 *Appl. Opt.* **53** 8514
[5] Ben X et al 2014 *Chin. Phys.* B **23** 099501
[6] Nicolas C et al 2013 *Opt. Lett.* **38** 2086
[7] Kristan P G et al 2014 *Opt. Lett.* **39** 3857
[8] Roshita D R et al 2013 *Opt. Express* **21** 4106
[9] Jordan D L et al 1996 *Appl. Opt.* **35** 3583
[10] Faouzi G et al 2006 *J. Quant. Spectrosc. Radiat. Transfer* **98** 13
[11] Jordan D L and Lewis G 1994 *Opt. Lett.* **19** 692
[12] Zhang H and Kenneth J V 2009 *Opt. Express* **17** 5217
[13] Jan K et al 2013 *Opt. Express* **21** 27032
[14] Shu J H et al 2009 *Chin. Phys. Lett.* **26** 024207
[15] Scott J T et al 2006 *Appl. Opt.* **45** 5453
[16] Born M and Wolf E 2002 *Principles of Optics* (London: Cambridge University Press) vol 1 chap 5 p 32
[17] Dennis G 2003 *Polarized Light* (Florida: Air Force Research Laboratory Press) vol 1 chap 24 p 480
[18] Jean-Jacques G et al 2002 *Nature* **416** 61
[19] Jan K et al 2012 *Appl. Opt.* **51** 6789
[20] Zhang J Q and Fang X P 2004 *Infrared Physics* (Xi'an: Xidian University Press) vol 1 chap 2.2 p 8